Journal of Engineering Science and Technology
Special Issue on Development of Sustainability Systems - I, 33 - 54

MECHANICAL VIBRATION INFLUENCE IN MICROSTRUCTURAL ALTERATIONS AND MECHANICAL PROPERTIES OF 304 STAINLESS STEEL WELD JOINTS

DAUOD S. DAUOD[1], MOHAMMED S. MOHAMMED[2, *],
ISRAA A.A. AZIZ[1], AHMED S. ABBAS[1]

[1]Production and Metallurgy Department, University of Technology, Baghdad, Iraq
[2]Training and Workshops Center., University of Technology, Baghdad, Iraq
*Corresponding Author: mohammed.s.mohammed@uotechnolgy.edu.iq

Abstract

This study investigated 304 stainless steel TIG welded joints with ER308L and ER310 fillers with and without mechanical vibration microstructural and mechanical properties variations. SEM and optical microscope were employed to analyze weld joints microstructure with and without vibration. Research results illustrated that welding with mechanical vibration decreases columnar 'dendrites number and length, and weld metal microstructure shifts from columnar to equiaxed dendrites. Decrease in dendrites average size from 547.42 μm to 64.32μm for ER308L weld metal and from 663.87 μm to 63.41 μm for ER310 weld metals dedicated in an investigation. Unmixed zone formation near the ER310 filler welding zone fusion line was observed in specific zones and disappeared with others. Dilution of welding zone metal reduced from 35.3 % without vibration to 29.7 % with vibration for ER308L and from 40.05 % to 36.02 % for ER310. The welding metal Ferrite amount for ER308L increased from 9% to 13% due to vibration, while ER310 decreased from 2% to 1%. ANSYS model for welding zone and HAZ of ER308L and ER310 fillers applied by Goldak model used to investigated effects of vibration on welding zone parameters and maximum welding heat to understand welding heat influence on welding zone and HAZ. Microhardness and tensile test results illustrated increasing tensile strength and decreasing hardness for the welding zone due to vibration effects.

Keywords: Ferrite percentage, Goldak model, Solidification mode; Unmixed zone; Vibration.

1. Introduction

304 stainless steel is one of the most widespread stainless-steel types because of its premium corrosion resistance, good formability and weldability, and application in industries like nuclear power facilities, chemical plants, petroleum and gas refineries, and biomaterials [1-4]. Despite all the above advantages, the lack of strength and hardness restricts some of this steel's applications. Many methods improve welded joints' mechanical properties; grain size refinement is essential for promoting strength and toughness [5]. Considerable weldment properties such as hardness, ductility, strength, corrosion resistance, toughness, and hot cracks susceptibility depend on weld metal solidification behaviour and resin ult microstructure [6-8]. Different techniques like nucleating agents' addition to molten weld metal, cool inert gas blowing to molten weld metal surface to stimulated surface nucleation, and arc oscillator, weld pool stirring, or arc plus pulsation work as external excitation changing weld metal microstructure grain size [7]. Previous research shows that electromagnetic or mechanical vibration through welding strongly contributes to welding zone grain refinement and affects dissolved elements redistribution across the weld pool, which controls hot crack susceptibility and trapped gas liberation in molten weld metal [8-10]. Compared with base metal, the welding zone suffers from lower mechanical properties because of weld metal dendritic solidification and segregation of alloying elements at high levels in 304 stainless steel plates, resulting in reduced mechanical properties [11]. The unmixed zone formation in dissimilar weldment weld line vicinity, which is caused by weld temperature variation between the base metal and weld zone, strongly influences corrosion resistance reduction [12]. Remove this area, and joint properties improvements can be achieved by applying electromagnetic vibration, as shown in earlier studies [13].

The weld metal vibration technique is widely used in welding. The vibration technique involves inoculants or nucleation agents' addition to the liquid weld metal during solidification. Like casting, inoculants' addition into the liquid weld metal promotes heterogeneous nucleation, resulting in excellent equiaxed grains solidifying metal. This research used 304 austenitic stainless steel welding joints with GTA technique der mechanical vibration synchronized with ER308L and ER310 fillers. Mechanical vibration applying effects on the three weldment joints' different zones microstructural changes (304 parent metal, HAZ, fusion line, interfaces, and weld metal zone), weld metal dilution amount and its effects on mechanical properties also the ability of produced weld joint with enhanced mechanical properties with this filler employing the mechanical vibration were evaluated. Many researchers compared electromagnetic vibration intensity and mechanical properties of welding zones. Still, previous researchers have yet to investigate the effect of mechanical vibration during welding processes on welding zone geometry dimensions parameters and its influence on dilution percentage between fillers and base metal. They investigated this alteration with dilution impacts in welding metal solidification mode and weldment mechanical properties.

The main objective of this paper is to investigate in detail the impacts of mechanical vibration in AISI304 SS weldments microstructure, solidification mode, ferrite percentage, residual stresses, and mechanical properties. very few researchers reported the mechanical vibration effects, and almost all earlier studies did not investigate all these properties together at one time. Also, the welding fillers used in this paper, ER308L and ER310 effects in welding zone microstructure and

its properties weren't investigated in this detail as the authors in this paper did, especially ER308L, a major of previous research employed ER309, ER310, or ER316. The vibration effects on welding heat distribution, maximum welding heat, and cooling rate were also investigated in this research with ANSYS models based on the double-ellipsoidal heat source Goldak model, which depended on welding zone dimensions. Alteration in these dimensions due to the vibration effects would be changing welding heat distribution and maximum welding heat in Ansys models, which improved these effects. The authors' literature review for previous research found only two papers studying these effects for the last ten years and proved it with ANSYS models.

2. Experimental Procedure

304 stainless steel sheet base metal with 4 mm thickness and 2.4 mm ER308L and ER310 filler wires diameter were applied. The chemical composition of base metal and fillers are shown in Tables 1 and 2. 304 base metal experimental samples with 10 × 15 cm dimension prepared. All joints were placed in butt joint configuration according to AWS D1.1 welding code. The welding procedure done with contemporaneous application of mechanical vibration produced from piezoelectric transducers can deliver mechanical vibration with 100 to 3000 Hz frequency range, as shown in Fig. 1. Four samples were welded in this study, two with 308L filler metals with and without vibration, and two with same procedures of ER310 filler. A mechanical vibration device is a transducer that transmits vibratory energy to experiment with a welding plate through a welding fixture. Vibration was produced based on a piezoelectric phenomenon that converts electrical signals into mechanical vibrations and vice versa [14]. Piezoelectric transducers are used as electromechanical sensors or actuators in various fields [15]. Most transducers use longitudinal vibration in the thickness direction of the plate or disc.

Table 1. AISI 304L base metal chemical composition.

C	Ni	Cr	Mn	Co	Si	N	Cu	Mo	Nb
0.02	8.1	18.4	1.4	0.09	0.4	0.05	0.01	0.2	0.01

Table 2. ER308L and ER310 filler's chemical composition.

Filler	C	Ni	Cr	Mn	N	Si	Cu	Mo	P
ER310	0.1	20.2	25.2	1.74	----	0.44	0.75	0.75	0.03
ER308L	0.01	9.81	20.1	1.71	0.03	0.50	0.1	0.72	0.03

Weld pool molten weld metal stirred by Lorentz force, induced by welding current interaction passing molten weld pool metal and transducers plate surface mechanical vibration. The welding process completed with direct current gas tungsten arc welding and electrode negative polarity (GTAW-DCEN). Welding process parameters illustrated in Table 3. For microstructure investigation, 20×10 mm specimens of base metal, HAZ, interface, and weld metal were prepared from welding zone samples. Welding microstructure investigation samples ground with silicon carbide paper of 1200 - 3000 grits and then polished by diamond paste to achieve mirror face surface, then three parts of HCL, two parts of acetic acid, 1-part HNO3 and two drops glycerol for 5 seconds etching solution used to microstructure examined of all samples. Optical and scanning electron (SEM) microscopies were employed for microstructural examination of weldments in different zones. Weld

metal ferrite number and amount obtained using the Feritscope FMP30 method and WRC 1992 diagram for stainless steel, Fig 2, respectively.

Table 3. Welding parameters.

GTAW	current	voltage	Welding speed	Protective gas	Electrode Dia.	Filler
W1	140A	11V	120 mm/min.	Ar 15 L/min.	2.4 mm	ER308L
W2	140A	11V	120 mm/min.	Ar 15 L/min.	2.4 mm	ER310

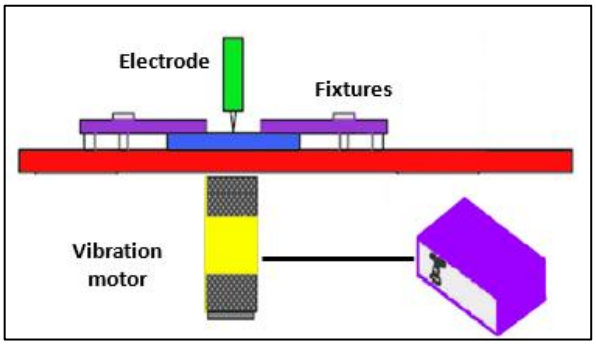

Fig. 1. Mechanical vibration system.

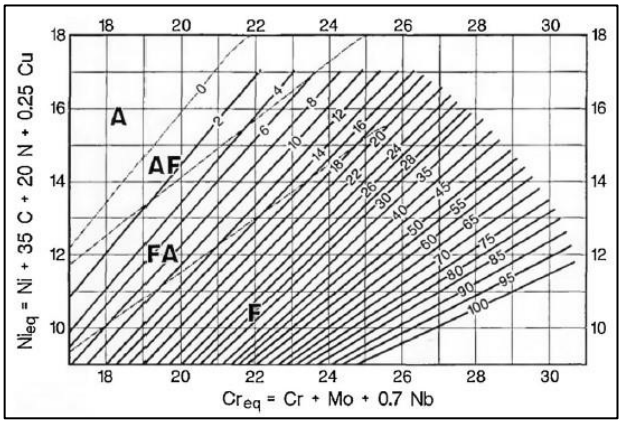

Fig. 2. WRC 1992 diagram for stainless steel.

3. Dilution Percentage

The mathematical equations in Eq. (1) and (2) are used to estimate the dilution between filler and base metal based on weld joints' geometrical characteristics [16], and Eq. (3) and (4) are used to calculate nickel and chromium equivalent in weld metal [17], where (AWD) is the weld deposit total area, (ATR) weld reinforcement area, (ARR) root reinforcement, (ABF) base metal fusion area, and finally, (ARG) root gap area, as schematically illustrated in Fig. 3:

$$AWD = ARG + ATR + ABF + ARR \quad (1)$$

$$\mathrm{DL}\% = (\mathrm{ABF}/\mathrm{AWD}) \times 100\,\% \quad (2)$$

Compositions of welding metal estimated from dilution calculations used in nickel equivalent (*Nieq*) and chromium equivalent (*Creq*) calculations employing the following equations [18]:

$$Creq = Cr\,\% + Mo\,\% + 0.7\,(Nb\,\%) \quad (3)$$

$$Nieq = Ni\,\% + 35\,(C\,\%) + 20\,(N\,\%) + 0.25\,(Cu\,\%) \quad (4)$$

Applying mechanical vibration during welding affects both dilution of weldments with filler metal and without filler metal addition. Compared with earlier studies, the dilution percentage decreased when welding was done under vibration because of the excitation appearing from vibration and high transfer of convection heat during vibration welding pool temperature decreased, lowering base metal melting temperature. Subsequently, welding metal dilution decreased by mechanical vibration because of vibration influence in dilution shifting to depress amount due to welding high heat transfer and decline in welding pool temperature [19, 20].

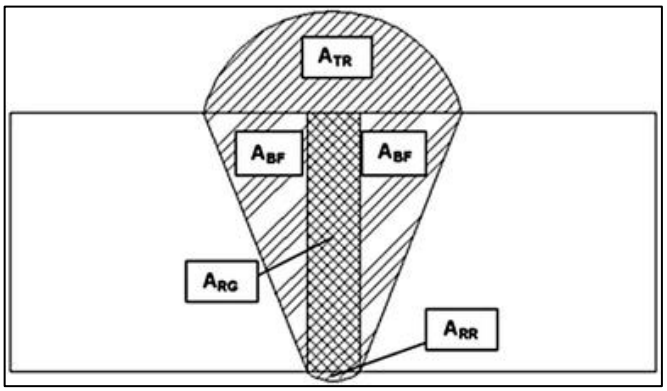

Fig. 3. Weldment joint dilution calculation schematic view sample.

4. Microstructure, Sem, Grain Size, and Ferrite Value

Metallurgical advanced microscope equipped with dual lights and polarizing darkfield + 5.0 MP digital camera and 40X-1600X magnification range - EQ-MM500T-USB type used in observing the weldments joints microstructure and estimate HAZ (heat affected zone) and welding zone grain size, ASTM E1382 code applied to evaluated and assessed the grains size from the optical micrographs by linear intercept method, software specialized in images analysing used to estimate these calculations. According to the ASTM code, five readings were marked, and the average was estimated. The FMP30 Periscope method was applied to calculate the Ferrite percent of welding zone samples in an average of ten assignments for each weld metal reported to ensure accurate measurements. SEM picture and EDS tests on specimens evaluate the weld metal microstructure details and elements migration. 304 welded samples cross sections prepared to measure the retained δ-ferrite amount. (ZEISS Axioskop 2MAT, OM) An optical microscope was used to observe the retained δ-ferrite with (Image-Pro Plus Ver. 5.0, IA) image analyzer to examine its phase fraction with vibration welding.

5. Vickers Microhardness

Base metal, HAZ, and weld metal specimens in flat positions were used in estimating microhardness across the three zones for each welded sample with a Vickers microhardness testing machine. Microhardness value measured with 0.98N load and 10 sec applied time at specimen surface cross-section quarter plane. Microhardness values were measured from the weld center line with a 0.5 mm shifting distance between measuring points on both sides. The microhardness test determined the hardness variation in the weld zone, fusion line, and HAZ with and without vibration for both fillers.

6. X-Ray Diffraction

(MACMXT-III, XRD) X-ray diffractometer device using Cu Kα radiation, 2°/min scanning rate with 40° to 100° and 2θ value, used to analyze AISI 304 weldments after welding with mechanical vibration: X-ray test operating voltage and current 40 kV and 30 mA.

7. Tensile Test

Tensile test specimens prepared by CNC machine with standard dimensions on the authority of ASTM E8 M-04 code as illustrated in Fig. 4. Smooth transverse edges of tensile test samples manufacturing for evaluated transverse tensile characteristics of gas mixtures welding joint. The specimens were tested with a 100 kN electromechanical controlled testing machine, and three readings were reported for each gas mixture sample.

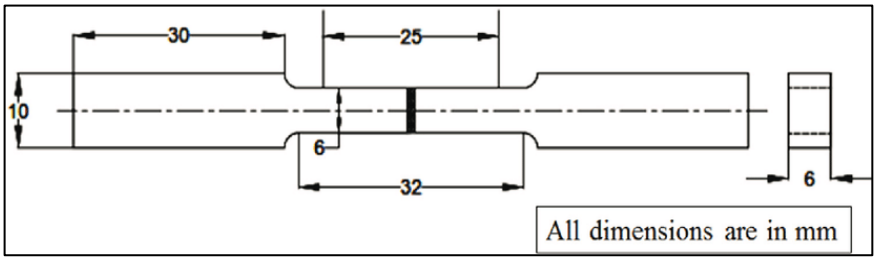

Fig. 4. Tensile test welded joint samples dimensions.

8. Results and Discussion

8.1. Dilution percentage

Weldments samples dilution calculations with ER308L and ER310 fillers weldments with mechanical vibration and without it and Nieqv and Creqv illustrated in Table (4). Results in Table (4) demonstrated that filler dilution decreased with automated vibration application. The welding pool temperature dropped and lowered parent metal melting because of rising agitation from mechanical vibration and high convective heat transfer. Therefore, the dilution of weld metal decreased when mechanical vibration increased, and dilution amounts reduced due to high heat transfer and falling in temperature of the welding pool [21].

Table 4. Welding metal Nickel and Chromium equivalents, dilution, and Creqv to Nieqv ratio with and without vibration.

Filler	Parameters	Without vibration	With vibration
ER308L	Cr_{eqv}	19.48	20.40
	Ni_{eqv}	11.62	11.7
	D	35.3	29.7
	Cr_{eqv} / Ni_{eqv}	1.67	1.74
ER310	Cr_{eqv}	23.41	22.54
	Ni_{eqv}	17.83	18.02
	D	40.05	36.02
	Cr_{eqv} / Ni_{eqv}	1.31	1.29

8.2. Microstructure

Austinite 304 stainless steel base metal microstructure is shown in Fig. 5(A). Microstructure illustrated austenite with coaxial grains with δ-ferrite precipitated on grain boundaries. Ferrite segregation agent elements during solidification and thermomechanical treatments drive ferrite formation [22]. Austinite 304 stainless steel ER308L filler weld metal without mechanical vibration is shown in Fig. 5(C). With vibration in Fig. 5(D), SEM picture of weld metal shown in Fig. 5(B) for weld metal with vibration, weld metal showed microstructure of austenite (γ) and ferrite (δ) existence after complete solidification process with room temperature in welded joints, two types of ferrites (δ) can observe in fusion zone (skeletal δ-ferrite and lathy) formed in austenite matrix. Weld metal microstructure image with ER308L and mechanical vibration showed the microstructure of austenitic grains boundaries ornamented with vermicular delta-ferrites, which appeared like gray zones with dendritic patterns. Welding metal samples without vibration showed the highest lathy δ-ferrite type concentration from weld samples with vibration; weld metal samples with vibration illustrated much more attention to skeletal δ-ferrite than weld metal samples without vibration; these results demonstrated the drop in welding heat concentration in weld metal because the vibration effect which lowering the heat in this zone [23]. Welding metal compositions of the two samples justified solidification mode from the WRC 1992 diagram; from this diagram, it can be observed that all welding metals samples with ER308L filler belong to (γ + δ) solidification zone. The weld metal Creq/Nieq ratio has essential effects in δ-ferrite formation. David et al. [24] research provides that when the Creq/Nieq ratio is less than 1.35, the solidification ends with austenite formation. When the balance exceeds 1.35, weld solidification will end with ferrite formation. Results in Table 4 clearly show that in welded metal joints with ER308L, the Creq/Nieq ratio is more than 1.35. According to these values, the welded metals would solidify in ferritic/austenite mode.

AISI 304 stainless steel solidified welding metal based on FA solidification mode is classified into two stages. Precipitation of the fundamental ferrite stage starts when dendritic ferrite is created directly from molten weld metal; when the solidification continuous and eutectic colonies appear among primary dendritic ferrite, the solidification reaches the sconed stage, which is called the three-phase reaction stage. In this stage, Cr and Ni constraints enriched between eutectic colonies and primary ferrite at the last of the solidified liquid region. It solidifies as austenite at the solidification end [25]. According to that, the weld metal solidification sequence is precipitating of primary dendritic ferritic from molten

weld metal, then the formation of cellular and columnar eutectic colonies in inter dendrite region starting when primary ferrite growth, then austenite phase precepted from molten welding metal and enforcement with Cr and Ni between eutectic colonies and primary ferrite. Weld metal solidification crack susceptibility strongly depended on the solidification mode and initial phase [4]. The WRC 1992 diagram was used in this study to predict the welding metal delta ferrite of ER308L and ER310 fillers. ER308L delta ferrite contents from WRC 1992 diagram were 9 % for weldment without vibration and 6.6 % for weldment with vibration, demonstrating good agreement with ferrite scope measurement. WRC 1992 diagram calculations indicated the FA solidification mode expected for ER308L solidified metal. According to this mode, dendritic δ-ferrite will form, then nucleation of austenite and growth will follow on ferrite grains boundary; when welding pool cooling continued, ferrite transforms to austenite and welding zone microstructure expected to be austenite with dendritic arms and δ-ferrite precepted in grains boundaries, Fig. 5(D).

Table 5. Amounts of ferrite number (FN) and ferrite percentage (F) for ER308L and ER310 weld metal with and without vibrations.

Filler	Parameters	Without vibration	With vibration
ER308L	FN	9	13
	F %	6.6 %	9.3 %
ER310	FN	2	1
	F%	2.22 %	0.73%

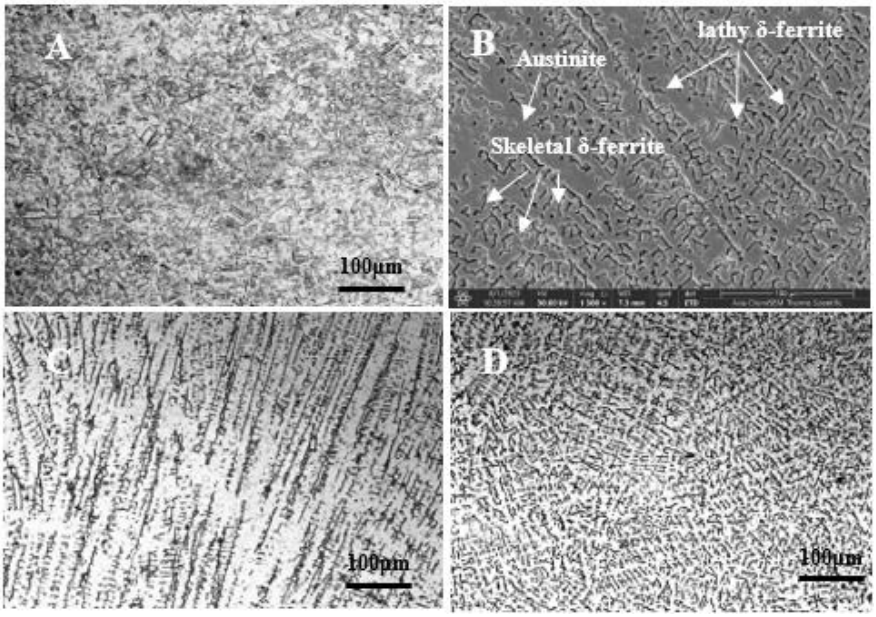

Fig. 5. ER308L welding zone microstructure.
(A) 304L base metal (B) welding zone SEM with vibration
(C) welding zone without vibration (D) welding zone with vibration.

Comparing microstructure microscopic images between welding metal with vibration and without revealed that mechanical vibration application resulted in microstructure grain refinement and formation of coaxial dendritic microstructure. This is due to the breaking up and fragmentation of controlled mechanisms in dendrite tips and arms of the solidification front line because resulted from vibration effects in the molten welding pool, which enhanced the nucleation rate and restricted the growth; this mechanism will reduce the G/N factor where G is grain growth, and N is the nucleation rate and producing fine grains weld metal microstructure [26]. This is due to the breaking up and fragmentation of controlled mechanisms at dendrite arms and tips in the solidification front due to vibration effects on the molten welding pool, leading them to increase the nucleation rate and restrict the growth.

The cooling rate would also increase with mechanical vibration applied by molten weld pool heat convection. Behavior like that would prevent significant dendritic structure creation. Also, due to the vibration, the weld metal solidification will go into the cooling zone, which acts as a nucleation site. However, due to the under-cooling effects, the dendrite tip fine fragmented will be more stable for all those refined grains microstructure expected in the weld metal zone with mechanical vibration. Due to the vibration effects, Ferrite amount increases, and ferrite uniform distribution in the weld metal microstructure can be detected. This is because of the average growth of coarse columnar dendrites in weld metal microstructure. Also, the solidified weld metal grains in weld pool boundaries would break down and solidify as a coaxial dendritic structure. The dendrite's length average measured from optical microscopy reduced from 547.42 to 64.32 μm by applying vibration. WRC1992 diagram and ferrite scope used to investigate mechanical vibration effect in weld metal ferrite percentage and dilution. Tables 3 and 4 revealed reduced dilution from 35.3 to 29.7 and increased ferrite number (FN) from 9 to 13 when welding with mechanical vibration. This increasing ferrite contained from the weld pool's high agitation and reduced welding temperature, increasing the cooling rate. This means δ-ferrite to austenite transformation time would not be enough to complete the transformation due to the vibration effects on the cooling rate. ER310 welding metal microstructure investigation revealed microstructure with fully austenitic matrix and δ-ferrite precipitated in grains boundary between austenite dendritic arms in small amounts, as illustrated in Fig. 6. Nickel and chromium equivalent amounts are shown in Table 4 for the welding metal of both fillers. According to the WRC1992 diagram and dilution percentage from the same table, the weld metal solidification mode was AF mode [11].

Feritscope measured ferrite amount was 0.73% with vibration and 2.22% without vibration, which agrees with weld metal dilution with base metal and with ferrite stabilize elements segregation such Cr and Mo in welding pool which pushing from solidified structure to dendrite arms space at solidification ending. Hence, AF solidification mode can be observed in small amounts in weld metal due to δ-ferrite formation in small quantities between dendritic arms, moving solidification orientation from A toward AF mode in these zones. ER310 weld metal shows different solidification modes when compared with ER308L weld metal. Also, the ferrite number acted in opposite behaviour, which levelled up because of vibration while lowering when vibration applied in ER310 weld metal; this is because Ni, Cu, C, and Mn elements are considered austenite stabilizers and had high concentrations in ER310 filler; as a result, microstructure of ER310

welding metal would be fully austenitic, as illustrated in Fig. 6. applied vibration effect on weld metal microstructure shown in Fig. 6(C). Due to the vibration, austenite grain size reduced and decreased δ-ferrite amount, resulting in Table 5 of ferrite scope measurements showing ferrite amount dropping from 2.22 to 0.73%.

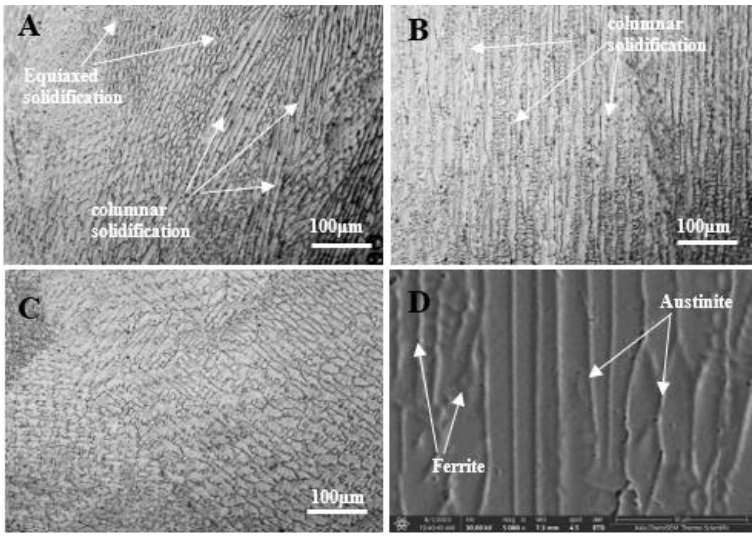

Fig. 6. Welding zone microstructure. (A) welding zone without vibration, (B) dendritic structure in welding zone without vibration, (C) welding zone with vibration (D) welding zone SEM with vibration.

Mechanical vibration improves convection heat transfer by improving molten metal moving between dendrite arms, decreasing welding pool temperature, and shortening solidification time. On the other hand, the number of broken columnar dendrites would increase from the welding zone fusion boundary toward the welding center line due to molten welding metal agitation from mechanical vibration. Weld pool temperature lowering resulted in stable nucleation sites, and new grains would be formed, which leads to coaxial dendrites formation and grain refinement [27, 28]. Weld metal microstructure image analysis showed decreased dendrite sizes from 663.87 to 63.41 by vibration. Also, the austenite-to-ferrite transformation would be hindered due to a higher solidification rate resulting from higher convection heat; this would reduce the δ-ferrite amount. Figure 7 investigated the base and weld metal interface; the microstructure image showed no crack or defect in the welding zone. Formation of unmixed zone revealed in welding zone due to difference in melting temperatures between AISI304 and filler metal. Unmixed area formation is more likely to exist in these conditions due to a match of melting points between base and filler metal and enough shortage in turbulence and unmixing elements gathering over a small area on the melting side. According to previous studies results, forming an unmixed zone lowers pitting corrosion resistance in dissimilar welds. Vibration contributes to the agitation of the molten welding pool to more turbulence; this would break many columnar dendrites, forming coaxial dendrites. Figures 7(A) and (B) illustrate this manifestation in the welding fusion line. Unmixed zone formation connected to the element's disturbance across the molten weld pool interface and penetration of

molten welding metal between dendrites. These facts are provided and reported by other researchers [22].

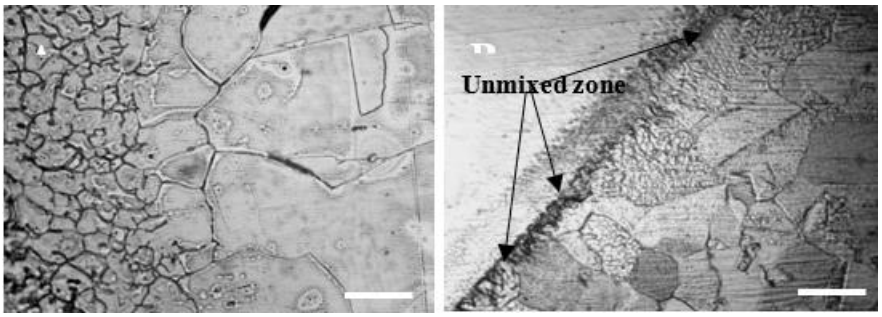

Fig 7. (A) ER310 welding interface and HAZ with vibration (B) ER308L welding interface and HAZ with vibration.

8.3. Retained δ-ferrite content

During weld metal solidification starting, primary δ-ferrite transformation to austenite. Finally, the retained liquid from this transformation also transformed into an austenite phase. Mechanical vibration during welding decreases the tendency of retained δ-ferrite to change in solidified weld metal and increase its content [29]. δ-ferrite phases are rich Cr phases in stainless steel, and γ-austenite as a high Ni percentage phase. Hsieh et al. research [30] showed that the δ-ferrite retained phase is a high Cr percentage phase and depleted Ni phases. Weld metal of stainless steel with chromium and nickel contained essentially solidified as austenite, which shows a strong tendency toward forming low melting phases and, in sequence, a strong trend towards welding zone hot cracks (solidification and liquation cracks). Weld metal in chromium-nickel stainless steel and high δ-ferrite solidification actively avoids hot cracks. Therefore, measurement of δ-ferrite is critical to improve stainless steel welding metal hot cracking resistance and to control the primary δ-ferrite crystals precipitation of molten weld metal during solidification.

ER308L welding zone morphology in Fig. 5 indicated two δ-ferrite morphologies, lathy and vermicular. At the same time, ER310 illustrated columnar and dendritic morphology. However, in general, 304L stainless steel welding metal solidification path follows this sequence: $L \rightarrow (L + \delta) \rightarrow (L + \delta + \gamma) \rightarrow (\delta + \gamma) \rightarrow (\gamma)$. As mentioned above, mechanical vibration during welding deeply affects liquid atoms' diffusion but simultaneously involves $\delta \rightarrow \gamma$ transformation subsequent cooling [31]. Solid phase $\delta \rightarrow \gamma$ transformation would occur during welding solidification, and based on Cr and Ni diffusion, a primary phase during $\delta \rightarrow \gamma$ phase transformation was δ-ferrite [32]. This is why the primary δ-ferrite affected the residual δ-ferrite morphology.

Figures 6(A) and (B) illustrate ER310 welding metal residual δ-ferrite morphology without vibration; continuous precipitation of residual δ- δ-ferrite can be indicated with columnar grain, forming a constant primary δ-ferrite morphology. Welding with mechanical vibration resulted in equiaxed grains, as shown in Fig. 6(C). These grains were not enlarged due to mechanical vibration, and many dendrites formed with equiaxed grains in weld metal; this complex microstructure would involve discontinuous morphologies of the residual δ-ferrite in some weld

metal regions, as shown in Fig. 6(C) and SEM morphology in Fig. 6(D). The primary δ-ferrite solidification major characteristic is residual delta ferrite presence found in weld metal structure after weld metal microstructure cooled down to ambient temperature. The weld metal chromium-nickel ratio is the factor responsible for primary δ-ferrite solidification. Welding metal dilution between base and filler material and alloying elements in weld metals also influence primary solidification processes during welding. Therefore, these factors must be considered when establishing the sequence to control primary δ-ferrite solidification of weld metals [33].

Inter-diffusion of Cr and Ni occur in δ-ferrite and γ-austenite during welding metal vibration due to variation between Cr and Ni concentration. Without vibration during welding, δ-ferrite retained phases only came from high Cr concentration zones. Controlled δ-ferrite formation resulted from insufficient Cr atoms diffusion time, so Cr was reserved in δ-ferrite during weld metal solidification. When welding is done with vibration, welding pool atoms move more rapidly, increasing the atom's diffusivity. Hence, Cr atoms needed sufficient time to diffuse, and the concentration gradient would decrease so that the retained δ-ferrite area decreased. Consequently, the content of δ-ferrite decreased. For these reasons, δ-ferrite contains an increase in ER308L when welding with vibration from 9% for weldment without vibration to 13% for weldment with mechanical vibration. This increase resulted from the vibration effect on lowering welding pool temperature and its impact on welding heat distribution, which didn't allow enough time for ferrite to transform into austinite, which increased the δ-ferrite in the weld metal. ER310 weld metal shows a decrease in residual δ-ferrite after vibration welding. The residual δ-ferrite decrement due to accelerated Ni atomic mobility during vibration, that is, mean Ni atoms diffuse within the austenitic matrix become easier than Ni combine with Cr to form δ-ferrite phase, this would result in δ-ferrite phase decreased in 304L stainless steel weld metal microstructures.

8.4. Vickers microhardness and tensile test

The relationship between vibration and hardness in 304L stainless steel welding is shown in Figs. 8 and 9. Maximum hardness without vibration was recorded at 193.8Hv and 201.2Hv for ER308L and ER310. Hardness maximum values with mechanical vibrator were 185.4Hv and 209.1Hv. Results above indicate that lowest hardness value with vibration and the highest values achieved without mechanical vibration in ER308L welding metal. The hardness value can be decreased by about 2.5% and 7.3% at vibration. The lower hardness value increment despite grain refinement during vibration welding resulted from the increasing of δ-ferrite in welding metal microstructure, which is softer than γ-phase. Lu et al. [34] reported that nucleation sites in welding metal can rise due to the vibration during welding, resulting in microstructure grain refinement and increased mechanical properties. On the other hand, hardness values increase with δ-ferrite content decreasing when vibration is applied because δ-ferrite is softer than γ-phase. Welded joint micro-hardness property improves with vibration welding due to reducing welding heat amount transferred to the weld zone, which caused an increase in the solidification rate of the welding zone, resulting in fine structure and high hardness values. But at the same time, decreasing solidification time will not allow enough time for δ-ferrite to γ-phase transformation, which results in high delta ferrite welding microstructure and affects the hardness value. ER310 weld metal without vibration

didn't show structure with refined grains or equiaxed microstructure, but as shown in Figs. 6(A) and (B) and explained above, had dendritic microstructure with discontinuous δ-ferrite resulted in low delta ferrite value and high hardness. The weld's metal center of weldment with vibration indicated equiaxed grains creation with many dendritic grains.

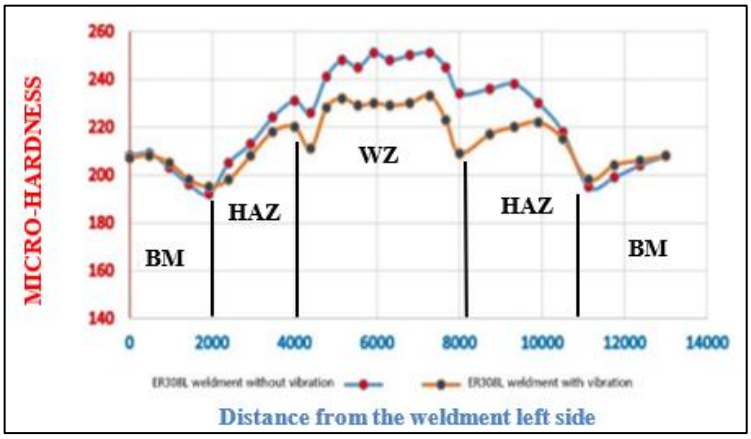

Fig. 8. ER308L weldment microhardness with and without vibration.

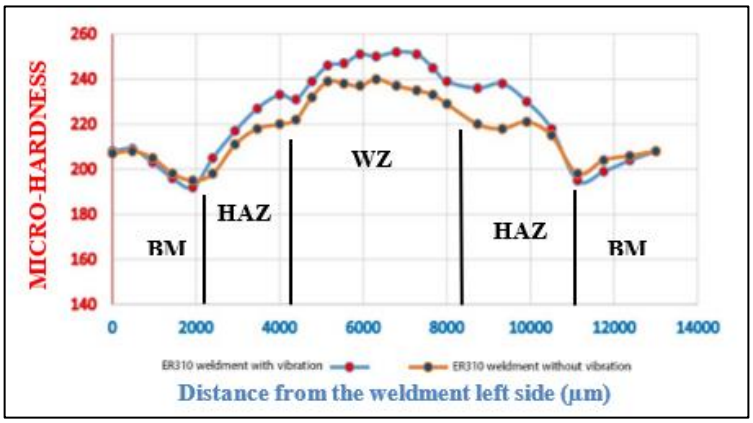

Fig. 9. ER310 weldment microhardness with and without vibration.

However, during vibration welding, molten pool perturbation motion occurred. This moving would break down the dendrites. At the same time, increasing nucleation happened due to the formation of these broken dendrites. On the other hand, temperature distribution would be uniform when welding with vibration, which means slight differences in temperature distribution [35]; therefore, the main effect of vibration in welding would be the welding temperature gradient (G). Wei's [36] research results show that flowing liquid metal can accelerate, and welding pool temperature can redistribute due to mechanical vibration. Hence, during solidification, the temperature gradient can decrease. At the same time, equiaxed grains are formed; welding molten metal nucleation points can be raised, and insufficient fine equiaxed grains formation would happen accompanied by hardness raising [37].

Tensile strength test results for all samples are summarized in Table (6). results clearly explain that tensile strength samples for both fillers without vibration show decreasing patterns while results of samples with vibration illustrated increasing tensile strength. The highest tensile strength value achieved 738 MPa for ER308L filler with vibration sample. Welding zone microstructure grain size changed due to the vibrations depending on changes in temperature distribution and maximum welding heat input. Without vibration, the welding zone cooling rate would become slower, giving more time for the ferrite to austenite formation. Also, HAZ grain structures would become coarser because the structure would be above austenite formation temperature for more time, resulting in dramatic grain growth. In addition, HAZ expanded without vibration due to the increasing welding heat. ER310 samples showed less tensile strength than ER308L due to the weld zone dendritic microstructure, dendritic structure results from austenitic weld metal rapid solidification. ER310 solidification weld metal with almost complete austenite or very low ferrite percentage resulted in high hardness, low elongation, and lower tensile strength in sequence. Vibration would influence the uniform distribution of welding heat and increase the nucleation rate, resulting in refined equiaxed grains microstructure.

Table 6. Tensile test results of welded joints ER308L and ER310 weld metal with and without vibrations.

Filler	With vibration	Elongation %	Without vibration	Elongation %
ER308L	698	15	683	13
ER310	642	11	621	10

8.5. X-Ray Diffraction Analysis

The diffraction pattern of weldment for ER308L and ER310 with mechanical vibration modes is indicated in Figs. 10(A) and (B). The pattern results of ER308L and ER310 show that δ-ferrite and γ-austenite were primary phases included in 304 stainless steel weldments but with very low δ-ferrite peak in ER310 pattern with almost complete γ-austenite microstructure. γ (111) diffracted peak had highest intensity with and without vibration for both patterns. Intensity ratio of γ (111) and γ (200) was 5: 1 without vibration in ER308L XRD pattern. However, γ (111) and γ (200), the intensity ratio was 2.5: 1 with a mechanical vibrator. FWHM width in γ (111), γ (200), γ (220), and δ (110) different crystallographic planes illustrated increasing due to vibration. Full width at half maximum (FWHM) was examined and calculated using Eq. (5) [38].

$$W^{\frac{1}{2}} = 2\sqrt{\frac{ln^2}{\pi}}\ (\frac{\lambda}{N.a}) \tag{5}$$

where λ is Cu target (nm) wavelength, N is the crystal cells' total number, and a is lattice constant. The crystal cells' total number (N) is small when lattice constant (a) is constant.

Therefore, it can consider crystal cells' total number as a primary factor of FWHM calculations. Due to the vibration effects, a distinctive increase in nucleation rate could be marked, resulting in grain refinement. That means when welding microstructure grain size decreased, crystal cells' total number (N) decreased, and FWHM would increase in sequence. Increasing nucleation rate resulted in crystal cells' growth retarding during the welding and higher FWHM

value. Kuo pointed out the increment of FWHM due to stacking fault after simultaneous welding vibration [39]. That means the stress relief mechanism for vibration welding is attributed to stacking fault formation. By monitoring the diffracted peak ratio, γ (200) intensity does not exceed γ (111) after vibration, but the diffracted peak ratio of γ (111) decreased vibration. Previous research pointed to the changes in the preferred orientation of crystallization direction during the $\delta \rightarrow \gamma$ phase transformation and strength resulting from that change due to 304 stainless steel welding vibration. Diffracted peak ratio for γ (111) closest packing FCC structure lowered with vibration. This, in sequence, would reduce the γ-austenite crystallization ability of the γ (111) plane.

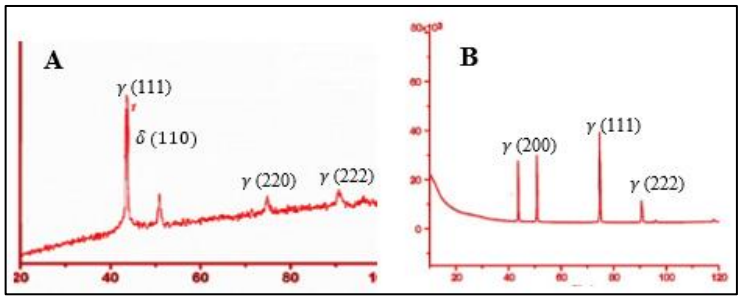

Fig. 10. (A) ER308L (B) ER310 welding zone XRD pattern with vibration.

8.6. Residual stress analyses

Regular welds without vibration usually lead to lattice distortion. They increased the residual stress due to rapid heating and cooling interaction, resulting in heterogeneous strain in solidified welding metal. Earlier researchers [40] inducted that residual stress plus alternate stress is the principle of vibration stress relief. Undistorted lattice in welding can be formed via dislocation slip when welding metal exceeds its yield stress; this procedure would produce strain relief action and residual stress. The microstructure examination and microhardness results indicated that the weld metal of both fillers had already deformed after the vibration, even when the alternate stress was minor. This meant that welded metal reached its yield stress value. Therefore, dislocation slipping occurred in welding metal due to vibration alternate stress plus welding residual stress, which is higher than welding metal yield stress. Then residual stress decreased due to the release of weld metal-constrained deformation. The micro-plastic deformation in weld metal began when the slip dislocation began, resulting from the alternate stress and residual cumulative greater than the yield stress. Thus, after dislocation slip, weld metal distorted lattice transfers into an undistorted lattice; this would decrease weld metal residual stress and strain energy. One of the most essential factors in vibration stress relief is vibration amplitude, which was discussed and provided by earlier researchers [41]. Still, this amplitude must be high enough to secure the required critical value and cause micro-strain because stress relief has limited value. The effect of stress relief could be lost when stress is reduced to determine value, even if vibration amplitude increases. Mathematical equation expressed the relationship between residual stress and vibration amplitude explained using Eq. (6) as follows:

$$\sigma r = 373.21\, e^{\left(-\frac{A}{1.006}\right)} + 113.61 \quad (6)$$

where σr is residual stress (MPa), A is vibration amplitude, and (V) is vibration amplitude.

By employing Wonzney and Crawmer [40] equations, which depend on the parameters of the diffraction methods to calculate the residual stress, diffraction angle 2Θ, and the known X-ray wavelength used to calculate the lattice spacing using Bragg's law. The precision necessary for strain measurement in engineering materials can be achieved using the diffraction peaks produced in the high back-reflection region in which 2 Θ > 120∘. The micro strain is determined from shifts, typically <1∘, of the mean diffraction-peak position. Residual stress can be expressed in Eq (7) as follows:

$$\sigma\psi = (E / 1 + v)\,(hkl)\;\; 1/d0\;(\partial\, d\theta\psi / \partial \sin 2\,\psi) \qquad (7)$$

where: σψ is residual stress, v: Poisson's ratio, E: Young's modulus, and d0: Stress-free lattice spacing, Residual stresses in ER308L welding metal reduced from 418 MPa to 164 MPa when welding with mechanical vibration and from 432 MPa to 177 MPa for ER310. These values pointed out that the weldment's residual stress efficiently decreased when applying vibration during welding.

8.7. Relation between tensile test results and ferrite content:

Ductile fracture mode pointed in all welded samples with and without vibration for both fillers shows no excessive hardening of the weld metal or heat-affected zone (HAZ). The UTS maximum value of a welded sample of ER308L filler welding sample without vibration was 531.7 MPa and 645.4 MPa with vibration, respectively. In comparison, the maximum UTS value of ER310 filler welding sample without vibration was 516.1 MPa and 601.7 MPa with vibration. These values satisfied the minimum requirement of AISI 304 stainless steel UTS, which must not lower 510 KN/mm^2. Thus, ER308L weldments with and without vibration show good solidification cracking resistance due to the (FA mode), according to WRC 1992 diagram. Also, δ-ferrite percentage in weld metal of this filler gives it very good solidification cracking resistance; the vibration during welding, as discussed above, would reduce, and redistribute the welding heat, inhibiting the formation of low melting phases, which influences the solidification cracks. ER310 filler weldments showed a marked decrease in UTS values for both weldments with and without vibration due to changes in solidification mode between the ER308L filler weldments and ER310 weldments, (AF) mode with ER310 illustrated microstructure with high possibility of solidification cracking and deficient δ-ferrite percentage which reduced the toughness of weldments. The UTS values for all the welded samples are acceptable and compatible with FN, Cr_{Eq}/Ni_{Eq}, welding metal solidification mode, and microhardness measurements.

8.8. Welding heat distribution model

ANSYS numerical simulation was used to estimate the welding temperature distribution from the molten pool crossing the HAZ, modify the heat source model, and understand the effects of mechanical vibration on the welding heat source. The geometrical model was generated with SOLID WORK software with the same experimental dimension mentioned in section (2) and then exported to ANSYS for completed heat distribution simulation. The material selected in ANSYS simulation was AISI304, mesh total nodes 68472, actual elements 41693 elements, and 0.05

mm element size, with medium refining. ANSYS heat distribution simulation is done by employing the Goldak model extension, which adds to ANSYS software, which is most commonly used for its high uniformity and is usually applied to arc welding simulation research; calculating the heat source model is essential in welding analysis simulations. Based on the above assumptions, numerical simulation used Goldak model equations in Eq. (8) and (9) to study the heat source. The boundary conditions for these equations are strongly related to the weld bead geometry and weld metal physical properties, as shown in Fig. 11.

Welding source power is calculated by using Eq. (10), and then welding pool or welding bead geometry parameters are measured for welding samples with and without vibration and loaded to the software with the other fixed parameters like welding speed, welding voltage, and number of welding passes to estimate the welding heat distribution model. No parameter in all ANSYS heat distribution models allows directly influencing process vibrations. Still, the alteration in weld bead geometry parameters between the welding samples with and without vibration reflected the vibration effects on heat distribution and, in sequence, on welding joint properties. The experimental results of this investigation had good agreements with the heat distribution model, the drop in welding heat due to vibration, and the dropping in welding heat accompanied by cooling rate dropping, which decreased the microhardness of the welding joint and HAZ for ER 308L as illustrated in Fig. 8. The microhardness curve in Fig. 9 shows an increase in microhardness with vibration for the ER 310 welding joint due to the vibration effects, producing uniform heat distribution and equiaxed fine microstructure. The uniform heat distribution means more heat convection and radiation from the weldment surface and more heat dropping. These results agree with the heat distribution model and give strong evidence about the model activity.

Microstructure images in Figs. 5, 6, and 7 illustrated excellent matching with heat distribution model. The alteration in microstructure patterns between weldments with and without vibration for both fillers cannot occur without a drop in welding joint and HAZ temperatures. The heat distribution model shows that dropping is proved by the alteration in microstructure due to the decreasing effects resulting from welding with vibration.

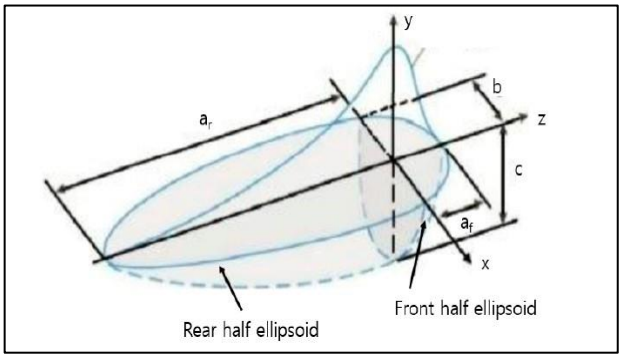

Fig. 11. weld bead geometry boundary conditions.

$$qf\ (x,y,z,t) = \exp\ (-3\ \left(\frac{(z-vt-z_o)^2}{af^2} + \frac{y^2}{c^2} + \frac{x^2}{b}\right)) \quad (8)$$

$$qr\ (x,y,z,t) = \frac{6\sqrt{3}f_rQ}{a_rbc\pi} \exp\ (-3\ \left(\frac{(z-vt-zo)^2}{ar^2} + \frac{y^2}{c^2} + \frac{x^2}{b}\right)) \quad (9)$$

where: V is the velocity of the heat source, Q is the effective heat energy (W), μ is the weld efficiency, V is the welding voltage, and I is the welding current. Q can be calculated from the following equation:

$$Q = \mu VI \tag{10}$$

Equations (8)-(10) show that the Goldak model's main parameters were not fixed but varied depending on welding conditions and geometry parameters. These parameters of the Goldak heat source model can be estimated by measuring the weld bead cross-section after welding tests. From Ansys model of welding samples according to Goldak model for ER308L with and without vibration, as shown in Figs. 12(A) and (B), for welding zone, fusion line, and HAZ, the variation in welding heat distribution and the maximum welding heat can be pointed, in Fig. 12(A) for weldments without vibration maximum welding heat in the welding center line was 1889.8 ºC and 1789.9 ºC for the same point with vibration as illustrated in Fig. 12(B), this decreasing in maximum welding heat indicated decreasing with weld zone geometric parameters resulted from the vibration effect on welding process.

The ANSYS model for ER310 filler weldment, shown in Figs. 13(A) and (B), demonstrated almost the same heat distribution pattern but with light increasing in maximum welding heat. The two fillers had nearly the same melting temperature and required the exact amounts of input heat during the welding, and theoretically, they must show the same heat distribution pattern, the authors explain the slight changes in welding zone geometric parameters between the two fillers which in sequence reflected on heat distribution Ansys pattern to the variation in alloying elements physical and metallurgical characteristics like the fluidity and its affinity to forms intermetallic compounds or phases between them, this variation was also the reason which resulted in changing the solidification mode from (FA) mode in ER308L weld metal to (AF) mode when welding with ER310 filler.

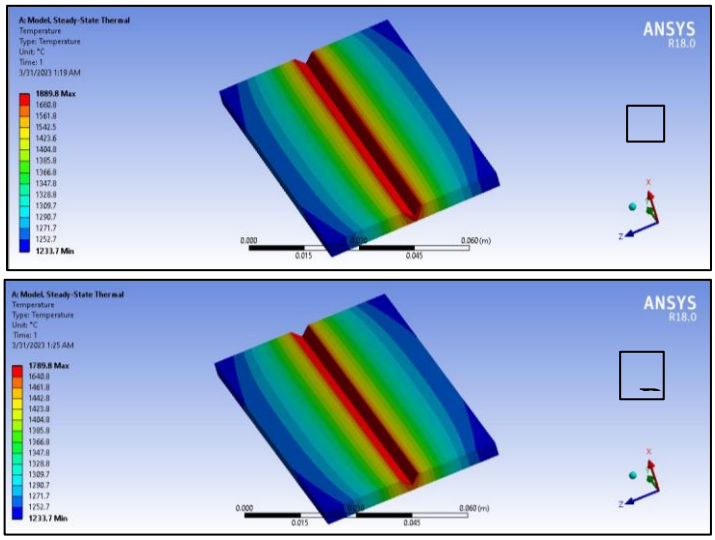

Fig. 12. ANSYS heat distribution model for ER308L filler welding zone and HAZ (A) without vibration (B) with vibration.

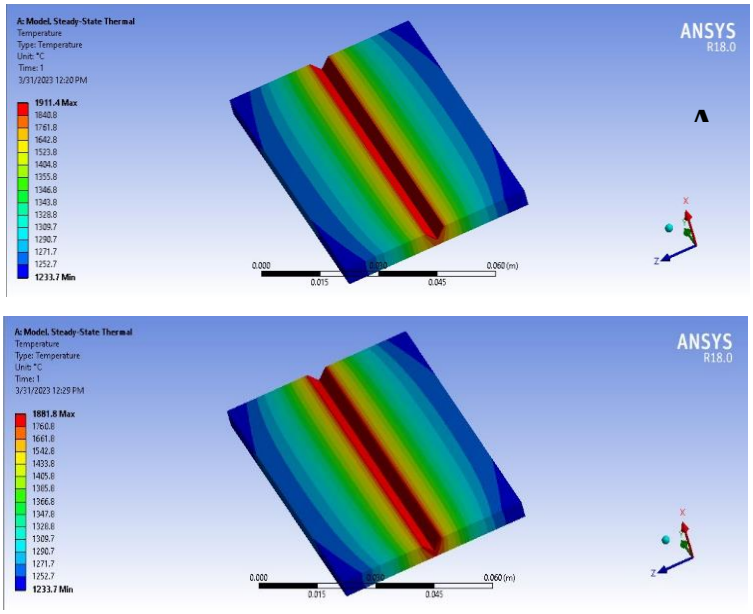

Fig. 13. Ansys heat distribution model for ER310 filler welding zone and HAZ (A) without vibration (B) with vibration.

9. Conclusions

Welding with vibration did not change the ER308L or ER310 weld metal solidification mode. The results illustrate that the solidification mode of ER308L welding metal was (FA) mode with or without vibration and (AF) for ER310 weld metal with or without vibration. Dilution between the filler metal and base reduction due to the vibration, which affects the δ-ferrite percentage in microstructure, dilution of ER308L reduced from 35.3 without vibration to 29.7 with vibration and from 40.05 without vibration to 36.02 with vibration for ER310 respectively. ER308L filler weld metal microstructure consists of an austenite matrix with ferrite (δ) existence; two types of ferrites (δ) can be observed in the fusion zone (skeletal δ-ferrite and lathy).

In contrast, ER310 filler weld metal microstructure revealed a complete austenite microstructure, and δ-ferrite precipitated with small amounts in the grain boundary and between austenite dendrites arms. Weld metal solidification of both fillers due to the vibration promoted the formation of refined coaxial grains with a much higher concentration of skeletal δ-ferrite in ER308L weldment and with the appearance of refined coaxial dendrites grains resulted from columnar dendrites breaking in ER310 welding metal.

Formation of unmixed zone detected ER310 welding zone due to differences in melting temperature between filler and base metal; at dissimilar joints, the construction of unmixed zone in the weld zone and base metal resulted from melting metal's laminar flow. Dendrite size decreased from 547.42 μm to 64.32 μm for ER308L weld metal and from 663.87 μm to 63.41 μm for ER310, respectively. Reduction in dendrite size for both fillers is achieved by vibration.

References

1. Pasupulla; A.P.; Agisho; H.A.; and Seetharaman, S. (2021). Characterization and analysis of TIG welded stainless steel 304 alloy plates using radiography and destructive testing techniques. *Materials Today: Proceedings*, 51(1), 935-938.
2. Ramakrishnan, A., Rameshkumar, T.; Rajamurugan G.; Sundarraju G.; and Selvamuthukumaran, D. (2021). Experimental investigation on mechanical properties of TIG welded dissimilar AISI 304 and AISI 316 stainless steel using 308 filler rod. *Materials Today: Proceedings*, 45(9), 8207-8211.
3. Kumara, K; Deheria, S.C.; and Manoj Masanta, M. (2019). Effect of activated flux on tig welding of 304 austenitic stainless steel. *Materials Today: Proceedings*, 18(7), 4792-4798.
4. Pandya, D.; Badgujar, A.; and Ghetiya, N. (2021). Effect of hydrogen additions to shielding gas on activated TIG austenitic stainless-steel weld. *Materials Today: Proceedings*, 47(4), 1025-1029.
5. Kumar, A.; and Dixit, P.K. (2020). Investigating the effects of filler material and heat treatment on hardness and impact strength of TIG weld. *Materials Today: Proceedings*, 26(2), 2776-2782,
6. Vinothkumar, H.; Balakrishnan, M.; Gulanthaivel, K.; Logeshwaran, R.; and Mohanraj, R. (2020). Investigation on effects of flux assisted GTAW welding process on mechanical, metallurgical characteristics of dissimilar metals SS 304 and SS 316 L. *Materials Today: Proceedings*, 33(7), 3191-3196.
7. Kumar, K; Kumar, C.S; Masanta, M; and Pradhan, S. (2021). A review on TIG welding technology variants and its effect on weld geometry. *Materials Today: Proceedings*, 50(5), 999-1004.
8. Kavitha, K.R.; Kumar, G.S.; Srinivas, G.L.; Mercy, J.L.; Sivashankari, P.; and Joy, N. (2021). Evaluation study of mechanical properties of dissimilar materials through TIG welding process. *Materials Today: Proceedings*, 44(5), 3894-3897.
9. Rhode, M.; Richter, T.; Schroepfer, D.; Manzoni, A.M.; Schneider, M.; and Laplanche, G. (2021). Welding of high-entropy alloys and compositionally complex alloys an overview. *Welding in the World*, 65, 1645-1659.
10. Ghazi, A.; Sabeeh, M.; and Salloum, A. (2022). Microstructure variation effects influence on characteristics and mechanical properties of Monel 400 and low alloy steel (ASTM 387-Gr.11) GTAW dissimilar joint. *Eastern-European Journal of Enterprise Technologies*, 5(12(119)), 13-20.
11. Mahajan, A; Singh, H; Kumar, S; and Kumar, S. (2022). Mechanical properties assessment of TIG welded SS 304 joints. *Materials Today: Proceedings*, 56 (5), 3073-3077.
12. Assefa, A.T.; Ahmed, G.M.S.; Alamri, S.; Edacherian, A.; Jiru, M.G.; Pandey, V.; and Hossain, N. (2020). experimental investigation and parametric optimization of the tungsten inert gas welding process parameters of dissimilar metals. *Materials*, 15(13), 4426.

13. Kumar, S.M; and Shanmugam, N. S. (2018). Studies on the weldability, mechanical properties and microstructural characterization of activated flux TIG welding of AISI 321 austenitic stainless steel. *Materials Research Express*, 5(10), 106524.
14. Manabendra, S.; and Dhami, S.S. (2019). Effect of TIG welding parameter of welded joint of stainless steel SS304 by TIG welding. *Trends in Mechanical Engineering & Technology*, 8(3), 1-4.
15. Jadhav, A.; and Wasankar, K.S. (2018). Optimization of process parameters of TIG welding for penetration and hardness of SS304 stainless steel weld. *International Research Journal of Engineering and Technology*, 5(10), 230-234.
16. Ha, X.H.; Jang, S.W.; Bang, W.H.; Yoon, S-U.; and Oh, K.H. (2002). Texture evolution in weld regions of SUS-304 stainless steel and trip steel. *Materials Science Forum*, 408-412, 1377-1382.
17. Kotecki, D.J. (2000). A Martensite boundary on the WRC-1992 diagram—Part 2: The effect of manganese. *Weld Journal*, 78, 346s-354s.
18. Dai, Q.X.; Cheng, X.N.; Zhao, Y.T.; Luo, X.M.; and Yuan, Z.Z. (2004). Design of martensite transformation temperature by calculation for austenitic steels. *Materials Characterization*, 52(4-5), 349-354.
19. Gosani, D.S.; and Kikani, P.T. (2016). effect of vibration in arc welding using SAE 1010 stainless steel. J*ournal of Emerging Technologies and Innovative Research*, 3(2), 17-20.
20. Lee, C.H. (2007). Formation of unmixed zone in the fusion boundary of dissimilar metal weld zone. *Journal of Welding and Joining*, 25(4), 1-3.
21. Mostafapour A.; and Gholizadeh, V. (2014). Experimental investigation of the effect of vibration on mechanical properties of 304 stainless steel welded parts. *International journal of advanced Manufacturing Technology*, 70, 1113-1124.
22. Savage, W.F.; Nippes, E.F.; and Szekeres, E.S. (1976). A study of weld interface phenomena in a low alloy steel. *Welding Research Supplement*, 55, 260-268.
23. Lake, F. (1993). Technical report: a new constitution diagram for predicting ferrite content of stainless-steel weld metals. *Materials & Design*, 14(6), 345-348,
24. David, S.A.; Vitek, J.M.; and Hebble T.L. (1987). Effect of rapid solidification on stainless steel weld metal microstructures and its implications on the Schaeffler diagram. *Welding Journal*, 66, 289s-300s.
25. Ma, J.C.; Yang, Y.S.; Tong, W.H., Fang, Y.; Yu, Y.; and Hu, Z.Q. (2007). Microstructural evolution in AISI304 stainless steel during directional solidification and subsequent solid-state transformation. *Materials Science and Engineering: A*, 444, 64-68.
26. David, S.A.; Babu, S.S.; and Vitek, J.M. (2003). Welding: solidification and microstructure, the journal of the minerals. *Metals & Materials Society*, 55 (6), 14-20.

27. Villafuerte, J.C.; and Kerr, H.W. (1990). Electromagnetic stirring and grain refinement in stainless steel GTA welds. *Welding Research*, 10, 1-13.
28. Kuo, C.W.; Lin, C-M.; Lai, G-H.; Chen, Y-C; Chang, Y-T.; and Wu, W. (2007). Characterization and mechanism of 304 stainless steel vibration welding. *Materials Transactions*, 48, 2319-2323.
29. Beraha, E.; and Shpigler, B. (1977). *Color Metallography*. American Society for Metals, Metals Park, Ohio.
30. Hsieh, C.C.; Lin, D.Y.; Chen, M.C.; and Wu, W. (2007). Microstructure, recrystallization, and mechanical property evolutions in the heat-affected and fusion zones of the dissimilar stainless steels. *Materials Transactions*. 48(11), 2898 - 2902.
31. Brooks, J.A.; Thompson, A.W.; and Williams, J.C. (1984). A fundamental study of the beneficial effects of delta ferrite in reducing weld cracking. *Welding Journal*, 63(3), 71-83.
32. Elmer, J.W.; Allen, S.M.; and Eagar, T.W. (1989). Microstructural development during solidification of stainless steel alloys. *Metallurgical Transactions A*, 20(10), 2117-2131.
33. Folkhard, E. (1988). *Welding Metallurgy of Stainless Steels*, 1st edition. Springer, Vienna.
34. Lu, Q.; Chen, L.; and Ni, C. (2007). Improving welded valve quality by vibratory weld conditioning. *Materials Science and Engineering A*, 457(1-2), 246-253.
35. Kuo, C-W.; Yang; S-M.; Chen, J-H.; Lai, G-H.; and Wu, W. (2008). Study of vibration welding mechanism. *Science and Technology of Welding and Joining*, 13(4), 357-362.
36. Wei, B. (1992). Unidirectional dendritic solidification under longitudinal resonant vibration. *Acta Metallurgica et Materialia*, 40(10), 2739-2751.
37. Hsieh, C.C.; Wang, P.S; Wang, J.S.; and Wu, W. (2014). Evolution of microstructure and residual stress under various vibration modes in 304 stainless steel welds. *The Scientific World Journal*, Article ID 895790.
38. Hsu, S. E.; and Wu, T. P. (1992). *X-Ray Diffraction Principles and Materials Structural Analysis*. 1st ed., 1-235, Materials Research Society, Taiwan.
39. Kuo, C.W.; Lin, C-M.; Lai, G-H.; Chen, Y-C.; Chang, Y-T.; and Wu, W. (2007). Characterization and mechanism of 304 stainless steel vibration welding. *Materials Transactions*, 48(9), 2319-2323.
40. Wonzney, G.P.; and Crawmer, G.R. (1968). *An investigation of vibrational stress relief in steel*. Defense Technical Information Center.
41. Dawson, R.; and Moffat, D.G. (1980). Vibratory stress relief: A fundamental study of its effectiveness. *Journal of Engineering Materials and Technol*ogy, 102, 169-176.